Applied Catalysis B: Environmental 183 (2016) 159–167

Contents lists available at ScienceDirect

Applied Catalysis B: Environmental

journal homepage: www.elsevier.com/locate/apcatb

Visible light photocatalytic activity for hydrogen production from water–methanol mixtures of open-framework V-doped mixed-valence titanium phosphate

Marco Serra, Herme G. Baldovi, Ferran Albarracin, Hermenegildo Garcia*

Instituto Universitario de Tecnología Química CSIC-UPV, Universidad Politecnica de Valencia, Av. De los Naranjos s/n, 46022 Valencia, Spain

ARTICLE INFO

Article history:
Received 26 July 2015
Received in revised form 8 October 2015
Accepted 12 October 2015
Available online 23 October 2015

Keywords:
Water splitting
Hydrogen production
Framework phosphate
Visible light photocatalytic activity
Mixed valence Ti^{3+}/Ti^{4+} titanium phosphate

ABSTRACT

Titanium dioxide is the most widely used photocatalyst for hydrogen production from water. Its main limitation consists in the lack of photocatalytic activity under visible light irradiation. One strategy to overcome this problem consists in using as photocatalyst Ti^{3+}-self-doped TiO_2 that presents an absorption in the visible range. In this context, we report the synthesis, characterization as semiconductor and photocatalytic activity under visible light or solar light irradiation of open-framework V-doped, mixed-valence titanium phosphate. These materials are characterized by an intense absorption spanning all the visible wavelength range caused by the presence of Ti^{3+} centers in equimolar ratio respect Ti^{4+}. This long wavelength absorption band allows the photocatalytic production of hydrogen under visible light irradiation. Suitable V-doping provides an additional charge separation level in the intra band-gap space that results in an enhancement of initial hydrogen production rate of a factor 5, reaching values of 47 $\mu mol/H_2\ h^{-1} g_{Ti}^{-1}$, in the absence of any noble metal as co-catalyst. Transient electron absorption spectroscopy has allowed to detect the state of charge separation in this phosphate that behave differently upon excitation in the UV or in the visible regions and whose intensity increases upon V-doping, reaching a maximum response at 0.5 wt.% in V. The flat band potential of the conduction band, measured by photocurrent as a function of the bias voltage, was estimated to be −0.10 V vs. NHE and the charge carrier density determined by impedance spectroscopy was 2×10^{20} carriers/cm^3.

1. Introduction

Titanium dioxide is the most widely used photocatalyst for pollutant degradation and also for hydrogen generation from water [1]. While TiO_2 has many desirable advantages as photocatalyst including affordability, lack of toxicity and stability, its main limitation is the lack of photocatalytic response under visible light irradiation [2–6]. As result of this, the overall efficiency of the photocatalytic activity of TiO_2 under sunlight irradiation is unsatisfactory and there is considerable room for improvement [2,7–14]. Among the different strategies to expand the photocatalytic response of TiO_2 toward the visible region including deposition of metal nanoparticles exhibiting surface plasmon band [15] and preparation of black titania [16], the most common approach has been TiO_2 doping by metal or non metal elements [3,17–20]. One possibility that has been recently studied has been self-doping of TiO_2 by Ti^{3+} forming blue colored solids [21] that had been reported to exhibit enhanced photocatalytic activity under visible light irradiation for hydrogen generation from water–methanol mixtures in the presence of Pt nanoparticles as co-catalyst [21].

There is a continuous interest in the development of new photocatalytic materials that can exhibit higher activity than TiO_2. In this context, we would like to report the photocatalytic activity for hydrogen generation of undoped and doped open-framework mixed-valence titanium phosphate. Open-framework refers to a non-porous crystalline structure with an atomic mass density below the maximum for bulk titanium phosphate (21 amu/nm [3] according to Ref. [22]). One of the advantages of framework metal phosphates as photocatalysts would be the flexibility in their synthesis, their stability in water, the availability of the transition metal and phosphate sources and their easy preparation in multigram scale. In this context, it has been recently reported that titanium phosphate can act as photocatalyst for hydrogen generation under UV light irradiation [28]. Also the synthesis of mixed valence Ti^{3+}/Ti^{4+} phosphate [$(Ti^{3+}/Ti^{4+})P$] octahedral–tetrahedral framework structure has been already reported [23]. In the present

* Corresponding author.
E-mail address: hgarcia@qim.upv.es (H. Garcia).

http://dx.doi.org/10.1016/j.apcatb.2015.10.027
0926-3373/

Table 1
Sample codes, composition and photocatalytic data for the mixed-valence (Ti^{3+}/Ti^{4+})P samples under study [a].

Sample	Metal composition (wt.%)		H_2 production (μmol)		Initial rate (μmol/h × g_{Ti})[b]
	V	Ti	6 h	24 h	
M1[c]	–	100	0.12	0.49	3.83
M2	–	100	0.23	0.71	9.57
M3	–	100	0.21	0.61	5.73
M4[d]	0.24	99.75	0.64	1.42	24.90
M5	0.54	99.46	0.96	1.79	47.89
M6	0.96	99.04	0.94	1.79	24.90
M7	2.32	97.68	0.62	0.63	15.32
M8[e]	–	100	–	0.02	0.055
M9[f]	0.48	99.52	0.14	0.31	9.21
M10[g]	2.1	97.9	0.14	0.2	8.98

[a] Irradiation conditions: 25 ml CH_3OH/H_2O (1:1) 25 mg catalyst reaction temperature 37–40 °C. A visible light LED was used as irradiation source (see Fig. S8 for emission spectra).
[b] Initial rate was estimated from the H_2 production at 1 h irradiation:
[c] Empirical formula of (Ti^{3+}/Ti^{4+})P compounds (M1–M7) is $Ti_{(2-x)}V_x(PO_4)(HPO_4)_2(H_2O)_2 \times (NH_2CH_2CH_2CH_2NH_2)_{0.5}$; the C content of M2 measured by combustion chemical analysis was 7.26%.
[d] The amount of V present in the material was determined by ICP.
[e] M8 corresponds to Ti^{3+}-doped TiO_2 rutile [21].
[f] M9 and M10 samples are two mechanical mixtures of M2 and V_2O_5 in different proportions similar to M6.

manuscript, we present characterization and photocatalytic data for hydrogen generation under visible light irradiation showing that mixed-valence Ti^{3+}/Ti^{4+} phosphates behave as semiconductors and photocatalyst. Herein, the flexibility in the preparation of open framework phosphates has been exploited for the synthesis of a series of V-doped titanium phosphates with enhanced photocatalytic activity. The state of charge separation upon irradiation has been detected and characterized by transient absorption spectroscopy and the flat band potential of the electron in the conduction band determined by photocurrent measurements against bias voltage. In spite of the high electrocatalytic activity for oxygen evolution of cobalt phosphate [24], it is surprising that only few reports are available on iron or titanium phosphate for the photocatalytic application and none of them refer to mixed valence Ti^{3+}/Ti^{4+} phosphate [25,28]. The present results serve to demonstrate the unforeseen behavior as semiconductor of mixed valence Ti^{3+}/Ti^{4+} phosphates, its activity as visible light photocatalyst and the versatility that this material offers for doping leading to the enhancement of its photocatalytic activity.

2. Materials and methods

2.1. Material preparation

(Ti^{3+}/Ti^{4+})P material was prepared as described by Ekambaram and Sevov [23]. Titanium metal (Alfa-aesar, 325 mesh) was mixed with 150 ml of an aqueous solution of 1,3-diaminopropane and phosphoric acid (molar proportion Ti 2: 1,3-diaminopropane 2.21:H_3PO_4 13.65:H_2O 500). The resulting mixture was stirred to achieve a homogeneous suspension and was sealed in a Teflon-lined autoclave. The autoclave was heated in an oven at 170 °C during a period varying from 1 day (M1), 2 days (M2) and 4 days (M3). After that time the suspension was cooled down to room temperature and the solid was filtered and exhaustively washed with water, ethanol and acetone. The samples were dried in vacuum at ambient temperature, and were stored under inert atmosphere. The V-doped samples (M4–M7) were prepared using the same experimental procedure except for the presence in the starting reaction mixture of an amount of vanadium metal (Alfa-aesar 325 mesh) mixed with titanium metal in weight proportion ranging from 0.25 and 2 wt.%. The amount of V present in the resulting materials was determined by ICP analysis. For the preparation of samples M4–M7 the autoclave was heated at 170 °C for 2 days. Higher or lower crystallization temperature and shorter or longer time should affect the crystal morphology of the resulting solid. In principle shorter or larger crystallization times should lead to smaller or larger particles sizes, respectively, and it could affect to the vanadium content and location in the solids [3]. (Ti^{3+})TiO_2 was prepared as reported by Feng and co-workers [21]. Briefly, 0.3 g of titanium powder was suspended in 10 ml of an aqueous solution of 2 M hydrochloric acid. The suspension was stirred to achieve homogeneity and was placed in a Teflon-lined autoclave of 25 ml. The autoclave was placed in an oven at 220 °C for 12 h. After this time the suspension was cooled to ambient temperature using an ice bath and was finally filtered and washed with water and ethanol. HRTEM images were recorded with a JEM 2100F JEOL 200 kV electronic microscope. UV–vis absorption spectra were recorded with a Jasco V-650 spectrophotometer. A Bruker EMX instrument was employed for the measurement of the EPR spectra with the following settings: frequency 9.803 GHz, sweep width 3489.9 G, time constant 40.95 ms, modulation frequency 100 kHz, modulation width 1 G, microwave power 19.92 mW. XPS of the samples were obtained in a SPECS spectrometer with a 150-MCD9 detector using MgKα ($h\nu$ = 1253.6 eV) X-ray radiation at an energy of 50 W.

2.2. Photocatalytic tests for hydrogen production

A suspension of the catalyst (25 ml, 1 g × l^{-1}) was sonicated for 10 min and placed in a closed reactor with an irradiation window of 12.56 cm^2 provided with temperature and pressure controllers. The reactor was placed in a thermostatic bath with a set point temperature of 25 °C. The temperature inside the photoreactor was measured by a thermocouple and reaches a stationary value between 37 and 40 °C. The suspension was purged with an argon flow of 2 psi for 15 min prior to irradiation. The photoreaction was performed from the top of the photoreactor by using a visible light LED with an irradiation spot of 4 cm^2 placed at a distance of 10 cm. The amount of hydrogen collected in the headspace of the reactor was analysed by injecting 100 μl in a gas chromatograph using a MOLSieve column, argon as carrier gas and a TC detector. Quantification of the amount of H_2 produced was performed based on a prior calibration using two gas mixtures having known H_2 proportions (standard 1:1% H_2, 3% ethane, 4% methane, 92% N_2; Standard 2:9% H_2, 1% (1,3-butadiene, propadiene, propane, propylene, ethylene and CO_2), 2% (ethane, methane and argon), 9% CO and 70% N_2). The absolute error of the measurement is 10 nmol of H_2 that is negligible in the present study.

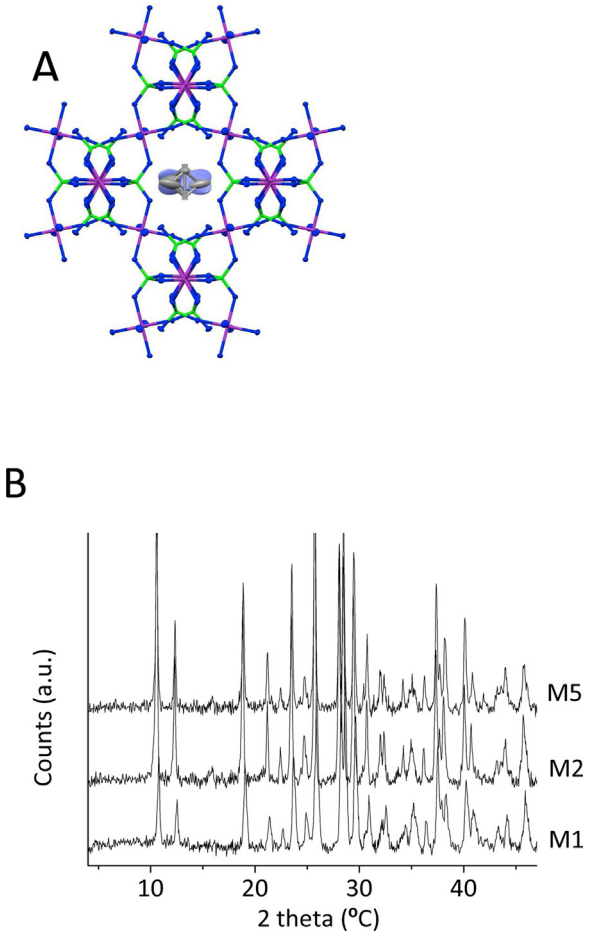

Fig. 1. (A) Crystal structure of the mixed-valence (Ti^{3+}/Ti^{4+}) P viewed along the *b*-axis. Purple atoms correspond to Ti, green to P, blue to O, grey to C and light blue to N. Hydrogen atoms are omitted for clarity. 1,3-diamine appears occupying disordered positions along *b*-axis channels (drawing generated by the program Mercury using the CIF data provided by Fachinformationszentrum Karlsruhe, Germany). (B) XRD patterns of the (Ti^{3+}/Ti^{4+})P samples (M1 and M2) and the V-doped (Ti^{3+}/Ti^{4+})P M5 (see Fig. S2 for the entire set of XRD patterns of the samples (Ti^{3+}/Ti^{4+})P M1–M3 and $(Ti^{3+})TiO_2$ M8) and Fig. S3 for the entire set of the XRD patterns of the V-doped (Ti^{3+}/Ti^{4+})P samples M2, M4–M7). (For interpretation of the references to color in the text, the reader is referred to the web version of this article).

2.2.1. Photocurrent measurements and determination of flat band potential of the conduction band

For photocurrent measurements, thin films of (Ti^{3+}/Ti^{4+})P were deposited on an FTO electrode ("Solaronix" $0.8 \times 10\,cm^2$). Deposition was performed by spreading a paste containing the semiconductor on the FTO surface using the doctor blade procedure. The surface of FTO was defined by adhesive tape. The paste containing the semiconductor was prepared in advance to the deposition of the film onto the electrode by dispersing 100 mg of (Ti^{3+}/Ti^{4+})P, 1 ml of acetone and 1 ml of α-terpineol. The suspension was stirred for 24 h to achieve a homogeneous dispersion. Then, acetone and α-terpineol were allowed to evaporate a room temperature to obtain the final dense semiconducting paste. After deposition of the paste, the adhesive tape was removed and the film of semiconductor on FTO was submitted to heating at 80 °C for 24 h increase the mechanical resistance of the layer. Photocurrent measurements were carried out using a 150 W Xenon arc lamp as a light source and a PTI model 101 monochromator. Electrical current was measured with an Amel 7050 potentiostat that was connected electrically to the FTO electrode with a platinum wire ("Trallero and Schlee") as counter electrode. The experiments were conducted inside a quartz cuvette (20 ml) that contained an aqueous 0.1 M KCl solution as electrolyte. The system was purged with nitrogen for at least 15 min before the measurement. Flat conduction band potential was determined by measurements of photocurrent applying increasing bias from 0.3 to 0.3 V (ref. Ag/AgCl) every 0.1 V (7 points).

Photocurrent onset was detected at 335 nm and the scan rate was of 2 min to stabilize, one of them without irradiation and the next minute with light. The number of charge carriers was determined using the same system connected to a frequency response analyzer. The experiment was carried from 0.5 V to −0.5 V each 0.1 V (10 points). At each voltage the system scanned in the frequency from 105 Hz from 0.1 Hz.

2.3. Transient absorption spectroscopy

Suspensions of (Ti^{3+}/Ti^{4+})P or doped (Ti^{3+}/Ti^{4+})P in acetonitrile were prepared by sonicating the powder for 10 min at 150 W in continuous mode in a bath-type sonication. The amount of solid was set to obtain an optical density at 266 of 0.35 units. The suspensions were persistent during the time needed for the transient absorption spectra measurements (about 3 h) without deposition of any solid. 3 ml of these acetonitrile suspensions were placed in a Suprasil quartz cuvette of $1 \times 1\,cm^2$ capped with septa. Suspensions were purged with argon or oxygen (for quenching experiments) for at least 15 min before the measurements. For ethanol quenching, an argon flow was bubbled through the suspension of (Ti^{3+}/Ti^{4+})P for at least 50 min before measurements. Transient measurements were carried out using the fourth (266 nm, 20 mJ/pulse) harmonic of a Nd:YAG laser (7 ns fwhp) as excitation source. The transient signal was recorded by the transmission mode using a 150 W Xenon lamp as monitoring beam through fibber optics to collect the transmitted light. The signal from the monochromator/photomultiplier detection system was captured by a Tektronix 2440 digitizer and transferred to a PC computer that controlled the experiment and provided suitable processing and data storage capabilities.

3. Results and discussion

Three materials (M1–M3) were synthetized varying the time of the hydrothermal synthesis from 1, 2 or 4 days (M1, M2, M3 respectively). Addition during the synthesis of vanadium metal in the required amount together with titanium metal powder results in the formation of V-doped mixed valence phosphates (M4–M7).

Table 1 summarizes the open-framework phosphate materials under study and their main analytical and physical data. For the sake of comparison we also include in the list a Ti^{3+} doped TiO_2 that was prepared according to the literature [21] through hydrothermal synthesis at 220 °C for 12 h starting from Ti metal and hydrochloric acid in aqueous solution. The main characteristics of this doped TiO_2 material (M8) are also included in Table 1. The success of the synthesis was confirmed by XRD (see Fig. S1 for indexation of XRD peaks and Table S1 for the 2θ value of M2, M4–M8). Crystallographic phase purity was assessed based on XRD that shows exclusively peaks that can be indexed as corresponding to the non-porous, open-framework (Ti^{3+}/Ti^{4+})P synthetized previously by Ekambaram and Sevov [23]. although we notice variations of the relative peak intensity. Fig. 1 shows the crystal structure of mixed-valence (Ti^{3+}/Ti^{4+})P and the XRD corresponding to the samples M1–M3 obtained at different times of hydrothermal synthesis, showing the same pattern in all cases, but differences in the relative intensity of the peaks. We also notice that the crystallinity of M3 obtained after four days of crystallization is significant lower than sample M1 and, particularly, M2. This could be due to a decrease in the average particle size of the crystals upon prolonged hydrothermal treatment or to a partial conversion of the crystals into amorphous materials. In any case, as it can be seen in Fig. 2

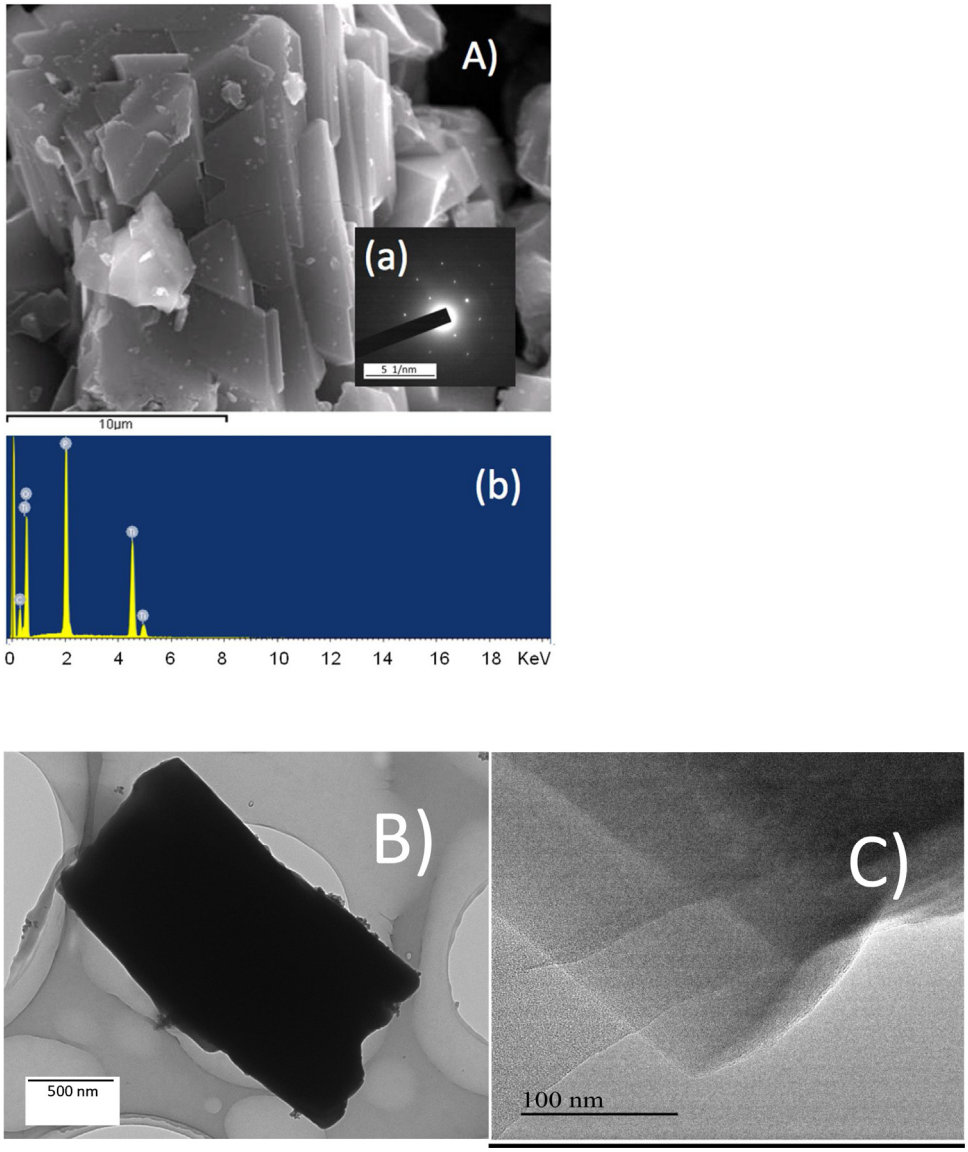

Fig. 2. (A) SEM image recorded for M2. Inset (a) electron diffraction image obtained by STEM (b) EDX analysis of the entire area of the sample. (B) and (C) TEM image of sample M2 at two different magnifications.

and Figs. S4 and S5 in the Supporting information the particle size of the undoped and doped (Ti^{3+}/Ti^{4+})P is very large about 8 μm.

The crystal structure of M1–M3 (see Fig. 1A) is constituted by TiO_6 octahedra and PO_4 tetrahedra sharing the edges. The lattice contains Ti—O—P, bonds but not P—O—P or Ti—O—Ti bonds. There is an equimolar proportion between Ti^{3+} and Ti^{4+}, the difference being that the octahedra around Ti^{3+} have two water molecules in trans position, while for Ti^{4+} the coordination sphere is occupied by six different phosphate units. The lattice defines channels along the *b*-axis in which 1,3-propanediamines are located occupying disordered positions along the channel.

In the case of V-doped (Ti^{3+}/Ti^{4+})P, XRD shows again that the samples M4–M7 are highly crystalline, without gradual shift or variation of intensity of the diffraction peaks observed for samples in where the vanadium content increases from 0.25 to 2 wt.%. Thus, XRD indicates that the samples should have the same structure commented earlier for (Ti^{3+}/Ti^{4+})P, except that some positions in the lattice should now be occupied by vanadium ions.

Scanning electron microscopy (SEM) images show that M1–M3 are constituted by aggregation of square-like flakes having a very smooth surface (Fig. 2A). In contrast V-doped samples M4–M7 are constituted by stack of well-defined particles without evidence of flakes. Particularly for M4–M7, well-defined prismatic crystallites of about 8 μm size can be observed (Supporting information Figs. S4 and S5). Samples M1–M7 also contain many much smaller particles without any defined geometry that can derive from degradation of larger crystallites. Electron diffraction of selected areas shows that the material is highly crystalline with well developed diffraction points of high intensity corresponding to a cubic packing in the crystal (see inset Fig. 2A). Due to the large size of the crystallites characteristic of the open framework phosphates and their lack of porosity, TEM images of samples M2–M7 are less informative than SEM (see Fig. 2B and C), they also confirm the morphology of the samples.

The homogeneous V distribution in the sample was confirmed by elemental analysis combined with SEM. It was observed that vanadium was present at the corresponding atomic proportion determined by chemical analysis even in areas of 100×100 nm [2], both in large crystals as well as in the very small debris. This homogeneous distribution and particularly the presence of vana-

dium in large crystals support the homogeneous V distribution as result of the isomorphic substitution in the structure of titanium by vanadium ion. As an example Fig. S4 shows the results of elemental analysis in selected area of a large crystal indicated in the SEM image as well as in some other selected points of the SEM image (Figs. S4 and 5).

Information about the framework position and oxidation state of V could be obtained by monitoring in EPR spectroscopy the signal corresponding to Ti^{3+}. EPR spectroscopy is a technique that allows specifically monitoring ions and species with unpaired electrons. Accordingly, M2 exhibits an intense signal due to the presence of Ti^{3+} ions. The lack of variation in intensity and shape of the signal of the EPR spectrum of M2 (see Fig. S6) compared with those of M4–M7 could be due to the relatively low amount of the V (up to 2.32%). On the other hand, the lack of observation of new EPR signal in M4–M7 compared to M2 seems to rule out the presence of V^{4+} in the material. In contrast, V^{3+} or V^{5+} are EPR silent and would not be detected by EPR spectroscopy.

The possible location of V ions in M4–M7 can also be addressed based on variation on the absorption spectra of these samples compared to M2 (Fig.3). In fact, one of the interesting properties introduced by the presence of Ti^{3+} ions is a broad absorption band in the visible peaking at around 550 nm. Fig. S7 shows the diffuse reflectance UV–vis absorption spectra for $(Ti^{3+}/Ti^{4+})P$ containing various vanadium doping levels (samples M4–M7). As can bee seen there, the general effect of vanadium doping is a decrease in the intensity of the visible band corresponding to Ti^{3+}, without varying the position of the absorption band. This could suggest that vanadium is replacing preferentially this type of Ti^{3+} ions. Assuming that the valence-conduction band of the material corresponds to the onset of the visible absorption band (about 800 nm), it can be estimated that the energy bandgap of M2–M7 materials is about 1.54 eV. However, we notice that depending on the oxidation state V may have or may have not d–d electronic transitions in the visible region overlapping the characteristic d–d transitions of Ti^{3+}. Thus, the trend observed in the UV–vis absorption spectra upon V-doping suggest not only replacement of Ti^{3+} ions, but also that the electronic configuration and oxidation state of the V–ions has to be compatible with the absence of absorption band in the visible region. V^{5+} having a d^0 electronic configuration would make compatible the lack of detection of EPR signals for V with the absence of d–d transitions in the visible region.

Fig. 3 also includes for the sake of comparison the absorption spectra of $(Ti^{3+})TiO_2$ rutile (M8). According to the literature [21], the main absorption band corresponding to the direct band gap transition has an onset wavelength of about 410 nm, considerably

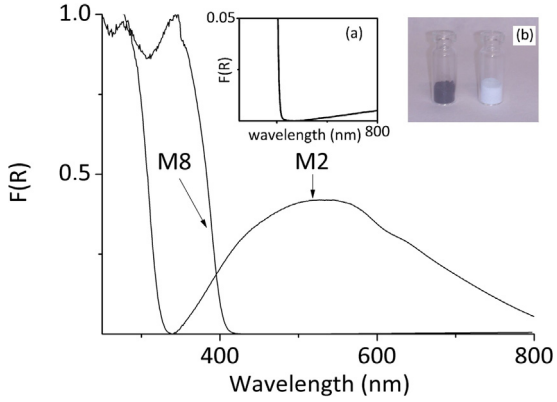

Fig. 3. Diffuse reflectance UV–vis absorption spectra (plotted as the Kubelka-Munk function of the remittance (R)) of the V-doped $(Ti^{3+}/Ti^{4+})P$ (M2) and $(Ti^{3+})TiO_2$ (M8) samples. Inset (a) Magnification of the of the M8 spectra; (b) Photo of the materials M5 (left) and M8 (right).

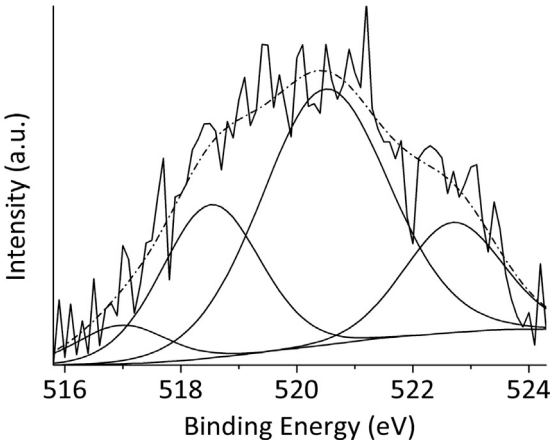

Fig. 4. XPS V $2p_{3/2}$ peak recorded for M5 and the best deconvolution to individual V^{5+}, V^{4+} and V^{3+} components (Note that V^{5+} has two components at 523 and 521 eV).

shifted with respect to the more intense band of M2 that absorbs below 330 nm deep in the UV region. The presence of some Ti^{3+} ions doping the TiO_2 rutile is also reflected by a weak absorption band in the visible (see inset of Fig. 3) that is responsible for the blue appearance of M8, but comparatively is of much less intensity than the visible bands recorded for M2–M7 samples.

Additional information about the oxidation state of vanadium in V-doped $(Ti^{3+}/Ti^{4+})P$ was obtained by XPS analysis of M5. Fig. 4 shows the high resolution V $2p_{3/2}$ peak together with the deconvolution of the experimental peak to three components corresponding to V^{5+}, V^{4+}, V^{3+}. From the best fitting of the experimental peak to individual components, the contribution of V^{5+}, V^{4+}, V^{3+} was estimated as 70, 24 and 6%, respectively. It should be, however, commented that under the conditions of XPS measurements partial reduction of higher oxidation state and some degradation of the mixed titanium phosphate can occur due to the low thermal stability of these materials. Thus, although XPS indicates that a large proportion of vanadium dopant must be as V^{5+}, the exact proportion value has to be taken cautiously.

Taking to account that the empirical formula of $(Ti^{3+}/Ti^{4+})P$ is $Ti_2(PO_4)(HPO_4)_2(H_2O)_2 \times (NH_2CH_2CH_2CH_2NH_2)_{0.5}$, it is likely that charge compensation due to the higher oxidation state to V with respect to Ti is achieved by the corresponding increase in the proportion of PO_4^{3-} respect to HPO_4^{2-} and/or by some vacancies in the $NH_2CH_2CH_2CH_2NH_2$ diamine cations present in the pores. Alternatively, charge compensation may include the presence of O = (most probably $V = O^{3+}$).

3.1. Photocatalytic hydrogen generation

As commented in the introduction, the present study is aimed at showing the photocatalytic activity of mixed-valence $(Ti^{3+}/Ti^{4+})P$ and the influence of V-doping. For this purpose we selected hydrogen generation from water–methanol mixtures as a test reaction to evaluate the photocatalytic efficiency of these materials, particularly in comparison with the activity of $(Ti^{3+})TiO_2$ rutile that can be considered as a reference photocatalyst.

Preliminary tests show that irradiation of TiO_2 with visible light in pure water did not show any hydrogen evolution. As expected in view of the literature data TiO_2 is also devoid of any visible light photocatalytic activity for this reaction. Even the $(Ti^{3+})TiO_2$ sample containing Ti^{3+} ions as dopant exhibits a negligible photocatalytic activity under these conditions. This lack of activity can be understood considering that the crystal phase of $(Ti^{3+})TiO_2$ is rutile that has been frequently considered much less active than anatase or than the combination of anatase with a low proportion of rutile

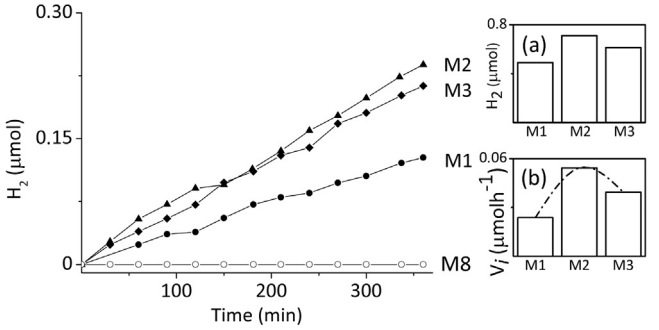

Fig. 5. Photocatalytic hydrogen production from water–methanol mixtures using M1–M3 samples as photocatalysts under visible-light irradiation. Experimental conditions: 25 ml CH_3OH/H_2O (1:1), 25 mg of photocatalyst, reaction temperature 37–40 °C. Inset (a) Hydrogen production at 24 h; inset (b) Initial reaction rate calculated at 1 h irradiation.

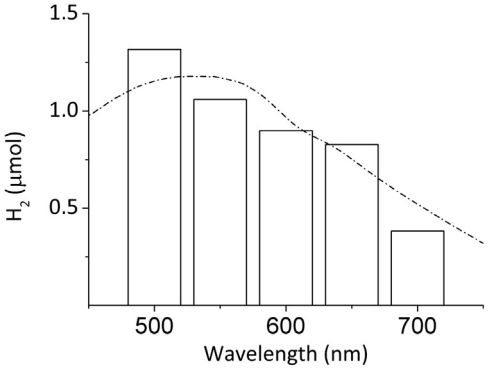

Fig. 7. Photoresponse of the V-doped (Ti^{3+}/Ti^{4+})P sample M5 under monochromatic visible light irradiation. The bars represent the amount of hydrogen accumulated in the head space of the reactor after 6 h irradiation. The dashed line corresponds to diffuse reflectance UV–vis absorption spectra of the material M5 plotted in arbitrary units. Experimental conditions: 25 ml CH_3OH/H_2O (1:1), 25 mg of photocatalyst, reaction temperature 25 °C.

(case of P25). In contrast, samples M1–M3 exhibit a significant photocatalytic activity for H_2 generation under these conditions using visible-light from a LED as irradiation source. To compare the catalytic activity of sample M1–M3 with the activity of other photocatalyst reported in the literature is has to be taken into account that in our case M1–M7 do not contain platinum as co-catalyst for hydrogen generation. Typically the reported photocatalytic activity of many semiconductors contain some noble metals to increase hydrogen production. While is well established that the presence of platinum increases the amount of hydrogen generated by a photocatalyst, due to the high cost of this precious metal it would be much convenient from the applicability point of view to avoid the use of platinum. According to Fig. 5 the most efficient photocatalyst both at 6 and 24 h with visible light irradiation (see Fig. S8 for the emission spectra of the LED employed as irradiation source) is the one obtained after two days of crystallization (M2). It is worth commenting that crystallinity does not appear to be a key factor in the present case since sample M3 that is less crystalline that M1 or M2 exhibit also a notable catalytic activity, higher than of sample M1.

Based on this data we selected 2 days as the optimal crystallization time for the preparation of other (Ti^{3+}/Ti^{4+})P samples and we performed a study of the influence of vanadium doping on the visible light photocatalytic activity of samples M4–M7. The results are listed in Table 1 and presented in Fig. 6. It was found that the photocatalytic activity of the undoped samples M2 increases, up to a factor of 5, due to the presence of vanadium as dopant element. If the initial reaction rate for visible-light hydrogen generation is plotted vs. V concentration a bell shape curve is obtained, indicating

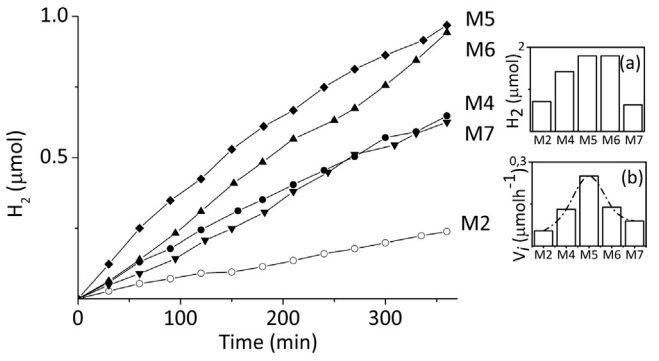

Fig. 6. Photocatalytic hydrogen production from water–methanol mixtures using M2, M4–M7 samples as photocatalysts under visible-light irradiation. Experimental conditions: 25 ml CH_3OH/H_2O (1:1), 25 mg of photocatalyst, reaction temperature 37–40 °C. Inset (a) Hydrogen production at 24 h (b) Initial velocity calculated at 1 h irradiation.

that there is an optimal V content of about 0.5 wt.%. In precedents in the literature studying the influence of doping on titanium dioxide and other semiconductors it has also been frequently observed that the presence of doping enhances the photocatalytic activity up to an optimal loading and then higher doping levels are detrimental for the photocatalytic activity [17]. This negative effect of increasing doping loadings has been attributed to an enhancement of charge recombination at the dopant elements for high dopant contents [27].

As commented when describing the XRD patterns, crystallinity of doped samples and, particularly, M5 was based on the coincidence of the diffraction peaks with that of undoped samples. However, it could be possible that the low percentage of vanadium could be present, at least partially, as an independent or separated phase.

In order to rule out conclusively that the enhancement the photocatalytic activity could derive from such a mixture of different materials in different phases, we also evaluated the photocatalytic activity for H_2 generation with visible light of two α-V_2O_5/(Ti^{3+}/Ti^{4+})P mixtures (M9 and M10) and the result are also included in Table 1 and Fig. S9. As can bee seen there, the photocatalytic activity and the initial rate of the V_2O_5/(Ti^{3+}/Ti^{4+})P is very similar of that of sample M2, and much lower than the photocatalytic series of sample M4–M7. These results are not surprising and can be interpreted as if the photocatalytic activity of the mixture derives from M2 the predominant component and as if the small portion of V_2O_5 does not make any contribution to the photocatalytic hydrogen generation. This poor catalytic activity exhibited by the V_2O_5/(Ti^{3+}/Ti^{4+})P mixtures that is similar to that of pure M2 speaks out against that the photocatalytic data shown in Fig. 6 and Fig. S9 could be due to the presence of V_2O_5 as independent phase and provide additional indirect support to the occurrence of doping in (Ti^{3+}/Ti^{4+})P materials.

The visible light photoresponse of the most active M5 sample was further confirmed by determining the hydrogen generation in the region from 500 to 700 nm using monochromatic light. The activity data under monochromatic light irradiation is presented in Fig. 7, where a comparison of the amount of hydrogen for each wavelength with the optical absorption spectrum shows that both properties follow the same trend.

The photocatalytic activity for hydrogen generation from water–methanol mixture was completed by evaluation of the activity of these materials under simulated sunlight irradiation. These conditions in which simulated sunlight is used as excitation source are closer the conditions for possible commercial application of the

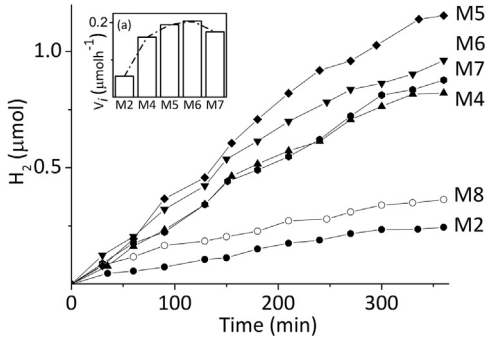

Fig. 8. Photocatalytic hydrogen production from water–methanol mixtures using M2, M4–M7 samples as photocatalysts under simulated sunlight. Experimental conditions: 25 ml CH_3OH/H_2O (1:1), 25 mg of photocatalyst, reaction temperature 37–40 °C. Inset (a) Initial velocity calculated at 1 h irradiation.

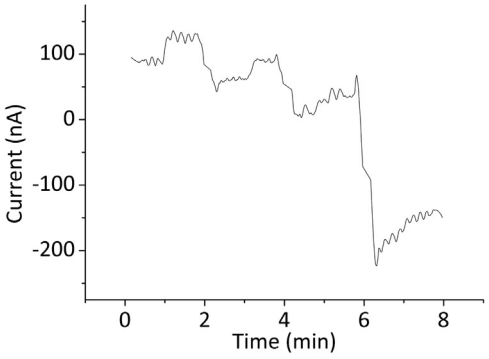

Fig. 10. Current vs. Time plot for sample M2. The bias voltage was scanned from −0.5 to 0.5 V, increasing 0.1 V every 2 min. The first minute after changing the bias voltage was in the dark and the next minute was illuminated with monochromatic 355 nm light from a Xenon arc discharge lamp.

material. As can be seen in Fig. 8 the order of the photocatalytic activity of M2, M4–M7 samples is the same as the one observed for visible light irradiation using a LED. The somewhat higher hydrogen amount generated using solar simulator is difficult to correlate with the visible-light photocatalytic activity by LED due to the different power and spectra of the two light sources. The main differences upon irradiation with visible or simulated sunlight is photocatalytic activity of M8 rutile that is devoid of photocatalytic activity upon LED irradiation, but exhibits a photocatalytic activity higher than M2, but still lower than V-doped $(Ti^{3+}/Ti^{4+})P$.

The issue of the long term stability of vanadium doped $(Ti^{3+}/Ti^{4+})P$ as photocatalyst was addressed by performing a prolonged irradiation experiments for one week using ten times larger volumes and photocatalyst. It was observed that during such a comparatively long time the amount of hydrogen increases linearly during the whole period of time, as shown in Fig. 9. Furthermore, at the end of irradiation the used $(Ti^{3+}/Ti^{4+})P$ was recovered and characterized by UV–vis spectroscopy, XRD and SEM microscopy (see Figs. S10 and S11 respectively). No significant changes with respect to the initial fresh sample were observed in the XRD diffraction pattern (Fig. S10) or in the morphology of the particles by SEM (Fig. S11) for M5 after seven days irradiation, indicating the stability of the V-doped, mixed-valence $(Ti^{3+}/Ti^{4+})P$ under operation conditions of the photocatalytic reaction.

Overall the photocatalytic data shown in Figs. 5–9 and Table 1, together with the availability of the synthetic precursors and the easy doping procedure show that $(Ti^{3+}/Ti^{4+})P$ are very promising visible light photocatalysts that offer many possibilities for

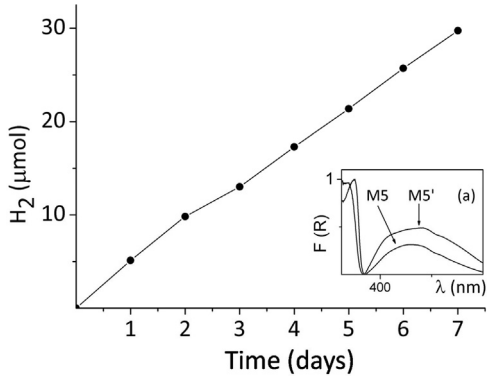

Fig. 9. Long-term photocatalytic hydrogen production from water–methanol mixtures using M5 sample as photocatalyst under visible-light irradiation. Experimental conditions: 250 ml CH_3OH/H_2O (1:1), 250 mg of photocatalyst, reaction temperature 38 °C. Inset (a) Comparison of diffuse reflectance UV–vis absorption spectra (plotted as the Kubelka-Munk function of the remittance (R)) of the fresh V-doped $(Ti^{3+}/Ti^{4+})P$ sample (M5) and the same sample used as photocatalyst during 7 days (M5′).

improvement. The obvious one that will be explored in further studies is the reduction of the average particle size and the deposition of metal nanoparticles that could act as co-catalysts in the process of H_2 evolution.

3.2. Characterization of $(Ti^{3+}/Ti^{4+})P$ as semiconductor

After having observed photocatalytic activity for mixed valence $(Ti^{3+}/Ti^{4+})P$ samples and in order to support on solid grounds the behavior of these materials as semiconductor, we performed photocurrent measurements to determine the flatband potential of electrons in the conduction band of this material as well as carried out the transient absorption spectroscopy study to detect the charge separation state and to monitor the kinetics and the quenching behavior of this transient state. By exciting the samples with monochromatic light at 355 nm and measuring the photocurrent as a function of the applied voltage, a flat band potential for the conduction band of −0.1 eV vs. NHE was determined for M2 sample (see Fig. 10). This potential is just about the one required for hydrogen generation, it is similar to the potential of electrons of the conduction band of TiO_2. Similar value (−0.13 eV) was determined for the conduction band of $(Ti^{3+}/Ti^{4+})P$ using impedance spectroscopy that also gives an estimation of the charge carrier density for $(Ti^{3+}/Ti^{4+})P$ as 2×10^{20} carriers/cm^3 (see Fig. 10, Figs. S12–S14). It should be, however, commented that the measurements of impedance spectroscopy were complicate by the fact that it is not possible to sinter the film of $(Ti^{3+}/Ti^{4+})P$ on the FTO electrode, due to the thermal instability of $(Ti^{3+}/Ti^{4+})P$ that it is known to decompose a temperature higher of 150 °C. In the present study, the films of $(Ti^{3+}/Ti^{4+})P$ were prepared by prolonged heating of the $(Ti^{3+}/Ti^{4+})P$ powder on FTO at 80 °C. Transient absorption spectra were recorded upon excitation in the UV (266 nm) or in the visible (532 nm) region. As we will show later, although the transient spectra recorded at these two excitation wavelengths are very broad, the remarkable differences in lifetimes and temporal profile of the signal indicate that the location of the electrons and holes are different depending on the excitation wavelength. We noticed that according to the absorption spectra of the samples these two irradiation wavelengths may correspond to excitation of two different chromophores in the $(Ti^{3+}/Ti^{4+})P$ samples, presumably irradiation to the $(Ti^{4+})/P$ ion chromophore or to the $(Ti^{3+})/P$ chromophore for the 266 and 532 nm, respectively (see Fig. S15). For the sake of comparison we have also included in the transient absorption spectroscopic study a sample of $(Ti^{4+})P$ (M11) [26].

Upon 266 nm laser excitation of $(Ti^{4+})P$ or samples M2, M4–M7 the same transient spectra consisting in a continuous absorption with similar absorptivity in all the spectral window was recorded (see Fig. 11 for the transient absorption spectra recorded for M2

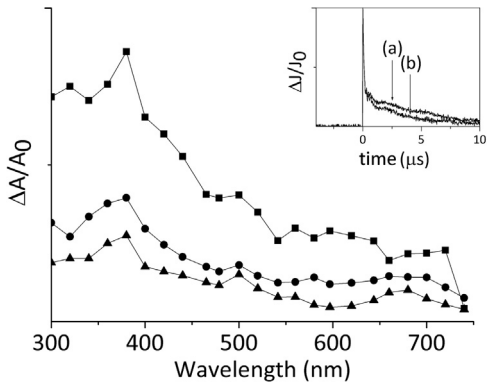

Fig. 11. Transient spectra recorder for an acetonitrile suspension of M2 upon 266 nm excitation recorded at 40 (■), 600 (●) and 1730 (▲) μs. The inset shows transient signal recorded for a N_2 purged acetonitrile suspension of M6 upon 266 nm excitation monitored at 400 (a) and 600 (b) nm.

coincident with the other samples). The temporal profile of the signal for each sample was coincident in all the spectral range (see for instance the inset of Fig. 11) without noticeable influence of V doping at the present doping levels. These temporal profiles consist in two regimes, one decaying very fast almost in the limit of our nanosecond detection system and accounting between 90 and 70% of the total intensity, a second time regime spanning from 0.12 μs to 10 μs. It is worth to comment that the transient spectra of these two regimes were identical.

As commented, vanadium doping of the sample has no influence on the transient spectra or temporal profile, but however, increases the intensity of the $\Delta J/J_0$ signal at zero time (data not shown). In order to give some evidence of the nature of the signal quenching experiments of the signal using oxygen (electron quencher) and ethanol (hole quencher) were performed.

Again the presence of oxygen or ethanol did not influence the transient spectra, but had a notable influence on the temporal profile of the signal, particularly in the faster regime. Oxygen increases the top $\Delta J/J_0$ signal by almost a factor 2 for M2 and 1.5 for M5. In contrast, ethanol decreases the top $\Delta J/J_0$ value in both cases, particularly, by a factor 1.5 for sample M5. This behavior is consistent with the transient absorption spectrum in the short life regime been dominated by holes, whose number will increase in the presence of oxygen by decreasing their recombination with electrons that will be removed by oxygen. When ethanol is present the signal decreases due to the quenching of the holes being monitored.

In the long time regime the influence of the presence of quencher is much smaller particularly for V-doped samples. This suggests that electrons and holes had been trapped at certain sites in the materials and they are less available to interact with quenchers. In fact a careful analysis of temporal profiles shows that the fast decay is followed by a minor growth of the signal that can be attributed to the relocation of the charge carriers in the materials. Importantly, the presence of vanadium at loading between 0.5–1 wt.% is reflected by a highest transient signal intensity, suggesting that the vanadium is also involved in the generation of electrons and holes.

The 532 nm laser excitation has some differences with respect to 266 nm. The first one is that (Ti^{4+})P does not exhibit any transient signal in accordance with the lack of excitation of this white powder that has not absorption band in the visible. In contrast, samples M2, M4–M7 exhibit transients whose spectra were similar for all samples consisting in a broad absorption in all the spectroscopic range with an increase in the absorbance from 450 nm to 300 nm. As an example, Fig. 12 shows the transient spectra recorded for M2. The temporal profile of the signal was also coincident in the whole spectral range and was similar for sample M2, M4–M7, the

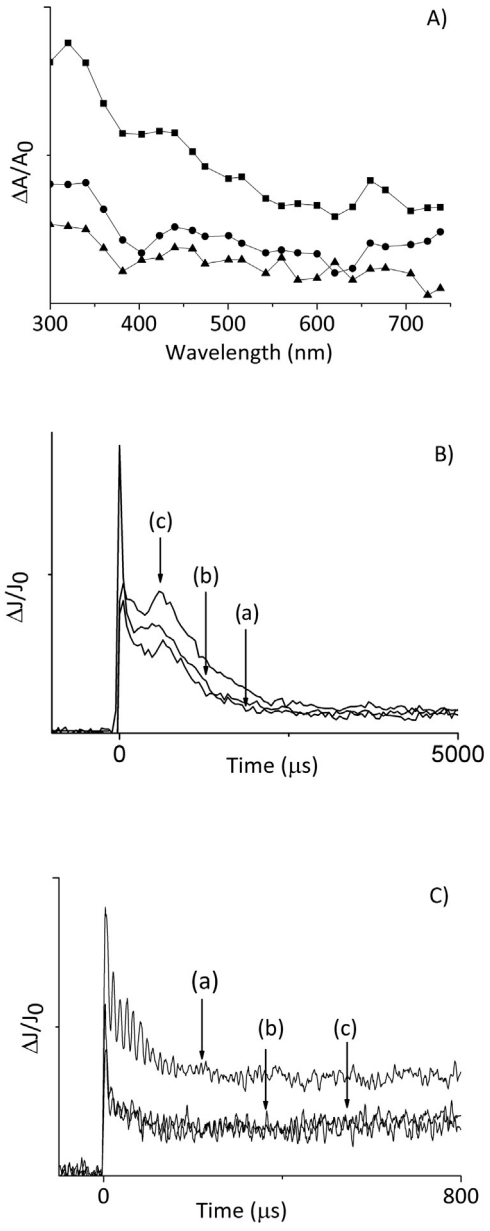

Fig. 12. (A) Transient spectra recorded for Ar-purged acetonitrile suspension of M2 upon 532 nm laser excitation monitorized at 40 (■), 60 (●) and 1730 (▲) μs. (B) Transient signal recorded for an acetonitrile suspension of M2 upon 266 nm laser excitation after purging the sample with Ar (a), O_2 (b) or CH_3CH_2OH (c). (C) Transient signal recorded for an acetonitrile suspension of M2 upon 532 nm laser excitation after purging with N_2 (a), O_2 (b) or quenching with CH_3CH_2OH (c).

most remarkable fact is now their extremely long lifetime, as Fig. 12 shows. As in case 266 nm excitation, also for 532 nm the temporal profiles have two regimes, one decaying very fast in a few μs that correspond between 50 and 20% of the total signal and a second regime having a very long lived signal, whose decay is not complete even four ms after the laser pulse. We attribute this extremely long life of the transient to the relocation of the charges in certain ions of (Ti^{3+}/Ti^{4+})P that should be significantly stable. It was observed, however, that the presence of oxygen and ethanol as electron and hole quencher, respectively, does not alter much the kinetics of the decay particularly in the long time regime.

Only the intensity of the signals are altered by quenching, reflecting that the interaction with oxygen of ethanol is a static quenching or take places at much shorter time scales. As an example Fig. 12 shows the quenching behavior of M2 with oxygen and

ethanol showing that only the intensity of the signal is affected (Fig. 12B and C).

The overall conclusion of transient spectroscopy is that there is a difference in the behavior depending of the excitation wavelength, indicating that excitation at the (Ti^{4+})P band (λ_{max} 280 nm) or excitation at the (Ti^{3+})P or (V)P leads to different location of electrons and holes. The influence, both at 266 and 532 nm excitation wavelengths, of vanadium doping in the transient consists in an increase of the signal corresponding to the charge separated state without affecting the spectra and the kinetics of the signal. In other words, spectroscopic evidence from the time resolved study indicate that vanadium ions can be excited at both UV and Vis wavelengths leading to electrons and holes, the larger efficiency in the generation of electrons and holes being reflected in a relative higher signal intensity for V-doped samples. In contrast there is no evidence for the involvement of V ions in trapping of the charge carrier that should be reflected probably in variation in the transient spectra or in the kinetics of electron-hole recombination (variation in the temporal profile) had been obtained. In summary, its that vanadium ions increases the population of electrons and holes (higher signal intensity either at 266 or 532 nm) without affecting to their relocation or their reactivity (same transient spectra as those shown in Figs. 11 and 1 for M2 and same temporal profile of the signal). Finally quenching, particularly by ethanol has been observed only for the 266 nm excitation and for the short (submicrosecond) time regime. According to this data, an increase of the efficiency of the (Ti^{3+}/Ti^{4+})P would be achieved if the charge carriers were more quenchable by methanol, that is employed in the photocatalytic hydrogen generation.

4. Conclusions

In the present manuscript it has been shown that easy-to-obtain, mixed-valence Ti^{3+}/Ti^{4+} phosphates, up to now ignored as photocatalysts, exhibit semiconductor behavior, with a conduction band reduction potential and charge carrier density similar to that of TiO_2. The state of charge separation generated upon light absorption can be detected by nanosecond transient absorption spectroscopy and is characterized by a broad absorption band spanning the entire spectral window. The decay of the signal has two time regimes, one predominant and fast (<0.15 μs) and other about 20% and slow (>10 μs). Vanadium doping increases the intensity of the transient signal without changing the spectra of the temporal profile.

This mixed valence Ti^{3+}/Ti^{4+} phosphate exhibits higher photocatalytic activity for hydrogen generation with visible light than that of TiO_2 reaching 50 μmol h^{-1} $g_{Ti^{-1}}$ in the absence of platinum as cocatalyst. The visible light photocatalytic activity derives from the presence of Ti^{3+} ions. In addition, mixed-valence phosphates can easily be doped by vanadium as supported by XRD. For the optimal V doping (0.5 wt.%) the performance of doped titanium phosphate was much higher than the intimate mechanical mixtures of vanadium oxide and (Ti^{3+}/Ti^{4+})P in similar weight proportions. The present manuscript therefore describes a new type of photocatalyst that combines easy preparation, flexibility in doping, visible light photoresponse in absence of noble metals and offers many possibilities to overcome titanium dioxide as photocatalyst.

Author contributions

MS synthesized the materials and performed the photocatalytic measurements. HGB measured and analysed the transient spectra. F.A. determined the flatband potentials. HG designed the work. The manuscript was written through contributions of all authors. All authors have given approval to the final version of the manuscript.

Acknowledgments

Financial support by the Spanish Ministry of Economy and Competitiveness (Severo Ochoa and CTQ20212-32315) and Generalidad Valenciana (Prometeo 2012/014) is gratefully acknowledged. M.S. thanks the Spanish CSIC and Technical University of Valencia for a postgraduate scholarship.

Appendix A. Supplementary data

Supplementary data associated with this article can be found, in the online version, at http://dx.doi.org/10.1016/j.apcatb.2015.10.027.

References

[1] (a) X. Chen, S.S. Mao, Chem. Rev. 107 (2007) 2891–2959;
(b) S. Girish Kumar, L. Gomathi Devi, J. Phys. Chem. A 115 (13) (2011) 211–13241.
[2] R. Asahi, T. Morikawa, T. Ohwaki, K. Aoki, Y. Taga, Science 293 (2001) 269–271.
[3] T. Ihara, M. Miyoshi, Y. Iriyama, O. Matsumoto, S. Sugihara, Appl. Catal. B 42 (2003) 403–409.
[4] H. Kisch, W. Macyk, Chemphyschem 3 (2002) 399–404.
[5] A. Primo, T. Marino, A. Corma, R. Molinari, H. Garcia, J. Am. Chem. Soc. 133 (2011) 6930–6933.
[6] S. Rehman, R. Ullah, A.M. Butt, N.D. Gohar, Hazard. Mater. 170 (2009) 560–569.
[7] K. Maeda, K. Teramura, D.L. Lu, T. Takata, N. Saito, Y. Inoue, K. Domen, Nature 440 (2006) 295.
[8] V. Balzani, A. Credi, M. Venturi, ChemSusChem 1 (2008) 26–58.
[9] S. Bensaid, G. Centi, E. Garrone, S. Perathoner, G. Saracco, ChemSusChem 5 (2012) 500–521.
[10] J.R. Bolton, Science 202 (1978) 705–711.
[11] G. Centi, S. Perathoner, ChemSusChem 3 (2010) 195–208.
[12] D. Gust, T.A. Moore, A.L. Moore, Acc. Chem. Res. 42 (2009) 1890–1898.
[13] N.S. Lewis, D.G. Nocera, Proc. Nat. Acad. Sci. 103 (2006) 15729–15735.
[14] N. Serpone, D. Lawless, R. Terzian, Sol. Energy 49 (1992) 221–234.
[15] C. Gomes Silva, R. Juarez, T. Marino, R. Molinari, H. Garcia, J. Am. Chem. Soc. 133 (2011) 595–602.
[16] X. Chen, L. Liu, P.Y. Yu, S.S. Mao, Science 331 (2011) 746–750.
[17] (a) C. Burda, Y.B. Lou, X.B. Chen, A.C.S. Samia, J. Stout, J.L. Gole, Nano Lett. 3 (2003) 1049–1051;
(b) L. Gomathi Devi, R. Kavitha, RSC Adv. 4 (2014) 28265–28299.
[18] K. Koci, K. Mateju, L. Obalova, S. Krejcikova, Z. Lacny, D. Placha, L. Capek, A. Hospodkova, O. Solcova, Appl. Catal. B 96 (2010) 239–244.
[19] S. Sato, R. Nakamura, S. Abe, Appl. Catal. A 284 (2005) 131–137.
[20] N. Serpone, J. Phys. Chem. B 110 (2006) 24287–24293.
[21] (a) F. Zuo, K. Bozhilov, R.J. Dillon, L. Wang, P. Smith, X. Zhao, C. Bardeen, P. Feng, Angew. Chem. Int. Ed. 51 (2012) 6223–6226;
(b) F. Zuo, L. Wang, T. Wu, Z. Zhang, D. Borchardt, P.J. Feng, Am. Chem. Soc. 132 (2010) 11856–11857;
(c) M. Liu, X. Qiu, M. Miyauchi, K. Hashimoto, Chem. Mater. 23 (2011) 5282–5286;
(d) L.R. Grabstanowicz, S. Gao, T. Li, R.M. Rickard, T. Rajh, D. Liu, T. Xu, Inorg. Chem. 52 (2013) 3884–3890;
(e) J. Su, X. Zou, Y. Zou, G. Li, P. Wang, J. Chen, Inorg. Chem. 52 (2013) 5924–5930.
[22] R. Murugavel, A. Choudhury, M.G. Walawalkar, R. Pothiraja, C.N.R. Rao, Chem. Rev. 108 (2008) 3549–3655.
[23] S. Ekambaram, S.C. Sevov, Angew. Chem. Int. Ed. 38 (1999) 372–375.
[24] M.W. Kanan, Y. Surendranath, D.G. Nocera, Chem. Soc. Rev. 38 (2009) 109–114.
[25] (a) X.J. Wang, H. Pang, S. Zhao, W. Shao, B. Yan, X. Li, S. Li, J. Chen, W. Du, ChemPhysChem 14 (2013) 2518–2524;
(b) K.M. Parida, D.P.J. Das, Photochem. Photobiol. A (2006) 68–72;
(c) D.P. Parida, Catal. Commun. 7 (2006) 68–72;
(d) K.M. Parida, N. Baliarsingh, D.P. Das, J. Mol. Catal. A 261 (2007) 254–261;
(e) K.M. Parida, D.P. Das, B.R. De, J. Mol. Catal. A Chem. 240 (2005) 1–6;
(f) K.M. Parida, D.P. Das, B.R. De, J. Mol. Catal. A 245 (2006) 217–224.
[26] Y. Liu, Z. Shi, Y. Fu, W. Chen, B. Li, J. Hua, W. Liu, F. Deng, W. Pang, Chem. Mater. 163 (2002) 561–567.
[27] L. Gomathi Devi, N. Kottam, S. Girish Kumar, J. Phys. Chem. C 113 (2009) 15593–15601.
[28] (a) S.Y. Guo, S. Han, B. Chi, J. Pu, J. Li, Int. J. Hydrogen Energy 39 (2014) 2446–2453;
(b) S.Y. Guo, S. Han, J. Power Sources 267 (2014) 9.